Phase Sensitive Detection in Modulation Excitation Spectroscopy applied to potential induced electron transfer in Cytochrome *c* Oxidase

Andreas Schwaighofer,[a] *Shelagh Ferguson-Miller,*[b] *Renate L.C. Naumann,*[a] *Wolfgang Knoll,*[a] *and Christoph Nowak*[a,c,*]

[a]Austrian Institute of Technology GmbH, AIT, Donau-City Str. 1, 1220 Vienna, Austria

[b]Biochemistry & Molecular Biology, Michigan State University, East Lansing, MI 48824, USA

[c]Center of Electrochemical Surface Technology, CEST, Viktor-Kaplan-Straße 2, 2700 Wiener Neustadt, Austria

The final version of this accepted manuscript was published in Applied Spectroscopy. DOI: 10.1366/13-07188.

ABSTRACT

Cytochrome *c* oxidase (C*c*O) from *R. sphaeroides* was investigated by Modulated Excitation Surface-Enhanced IR-Absorption Spectroscopy (ME-SEIRAS). Sequential electron transfer (ET) within C*c*O was initiated by electrochemical excitation. During modulated excitation by periodic potential pulses with frequencies between 20 Hz and 500 Hz, time-resolved IR spectra were measured by the Step-Scan technique with time-resolution in the millisecond time range. Conformational changes of the protein structure as a result of ET lead to rather complex SEIRA spectra with many overlapping bands embedded in a broad background signal. Phase sensitive detection (PSD) was used to separate single components within the broad band of overlapping structural bands in the amide I region. PSD is able to extract the periodic response of single components with the same frequency as the excitation from noise or from static background and therefore enhances the signal-to-noise ratio. Moreover, PSD enables validation of the fit model utilized for the deconvolution of overlapping bands by analyzing phase lags of single components acquired at different stimulation frequencies. Phase lags between the evaluated vibrational components and the modulated excitation increase with increasing excitation frequencies, which is an inherent prerequisite of this evaluation method.

Index headings: FTIR; Fourier transform infrared spectroscopy; SEIRAS; Surface-enhanced infrared-absorption spectroscopy; PSD; Phase sensitive detection; C*c*O; Cytochrome *c* oxidase; Band deconvolution; Modulation spectroscopy.

INTRODUCTION

Phase Sensitive Detection (PSD) had been found to be a very effective technique for sensitivity enhancement in combination with modulation spectroscopy. In the present work, modulated excitation Fourier transform infrared (ME-FTIR) spectroscopy is performed on C*c*O and the sequential ET within the protein is initiated by electrochemical excitation.[1,2] This method offers the possibility of modulating the excitation signal and measuring FTIR spectra in a large frequency range, particularly when used in combination with the Step-Scan technique. In earlier works, it has been demonstrated that the induced electron reaction is reversible and therefore suitable for modulated excitation experiments.[2] Conformational changes in protein secondary structure as a consequence of ET lead to SEIRA spectra with many overlapping bands embedded in a broad background signal. The goal of this work is to identify significant components within the amide I region using phase sensitive detection (PSD).[3,4] This method selectively highlights periodically changing signals stimulated by an external parameter, such as temperature,[5,6] pH,[4,7] concentration,[8,9] electric field,[10,11] pressure,[12] mechanical force,[13] radiant power[14] or absolute configuration.[15,16] PSD acts as a software lock-in amplifier and can be used in ME-FTIR spectroscopy without the need of any additional expensive hardware.[3,5] It can be applied offline after that the spectra have been obtained, which avoids complicated phase corrections and shortens the measuring time during data acquisition. Application of PSD converts the recorded tr-absorbance spectra into phase-resolved spectra and thereby (i) suppresses almost all frequency components of the noise and any constant background absorption and (ii) permits the selective detection of signals that show the same frequency as the stimulation. The resulting background compensation and the signal-to-noise ratio (SNR) are considerably better than those obtained by conventional difference spectroscopy. In particular, the characteristic increase of the phase lag with increasing excitation frequency permits the exclusive identification of components affected by

stimulation. Due to this inherent validation, spectra evaluation by PSD is considered to be more confident than evaluation by first-order derivatives or Fourier self-deconvolution (FSD), that significantly depends on the operator choice of two parameters.[5]

Fourier transform infrared (FTIR) spectroscopy has been proven as a powerful method for investigating protein dynamics. With its high sensitivity and characteristic marker bands for many molecules, IR spectroscopy provides a label-free environment for the investigation of molecular interaction and structural changes. In particular, time-resolved (tr-FTIR) methods promise to elucidate structure-function relationships even of large multi-redox center proteins such as the cytochrome *c* oxidase (C*c*O).[17-26] C*c*O is the fourth complex in the respiratory chain and is well characterized by FTIR methods; hence it poses an excellent model system for the present work. Our group established a method to immobilize membrane proteins in a biomimetic membrane system on an ATR crystal coated with a two-layer gold surface.[27] Incorporation of the protein in this protein-tethered bilayer lipid membrane (ptBLM) enables its investigation in a biomimetic environment that corresponds as closely as possible to the biological plasma membrane.[28] Direct electron injection into C*c*O has been shown to result in electron transfer (ET) along Cu_A/heme *a*/[heme a_3-Cu_B], the natural sequence of redox centers in the cytochrome *c* oxidase.[29] Induced electron transfer into C*c*O by electrochemical excitation has been investigated by fast-scan voltammetry and potentiometric titration followed by surface-enhanced IR-absorption spectroscopy (SEIRAS).[1,2,30] Employing electrochemical excitation, modulation can be achieved by application of periodic potential pulses, thus permitting a large variety of modulation amplitudes and frequencies.

The aim of this work is to demonstrate the convenient application of Phase Sensitive Detection to the amide I band in the FTIR spectrum of C*c*O to identifiy structural components that are involved in electron transfer through this large electron complex. To the best of our

knowledge, PSD has been applied to this extent only to relatively small and simple molecules and proteins before.

EXPERIMENTAL SECTION

Solvents and Chemicals. Purified water was obtained from a Sartorius-Stedim system (Göttingen, Germany) with a resistivity of 18 MΩ cm. Argon (purity: 4.8) and oxygen (techn.) gas were obtained from Linde Gas GmbH (Stadl-Paura, Austria). Bio-Beads (20-50 mesh) were purchased from Bio-Rad Laboratories GmbH (Munich, Germany). 1,2-diphytanoyl-*sn*-glycero-3-phosphocholine (DiPhyPC, >99%) was provided by Avanti Polar Lipids (Alabaster, AL, US). Dodecyl-*β*-D-maltoside (DDM, ≥98%), was purchased from Sigma-Aldrich (Steinheim, Germany). All chemicals were used as purchased.

Preparation of the two-layer gold surface on the ATR crystal. Preparation of the ATR crystal was done as previously described.[11,27]

Immobilization of the protein. C*c*O was immobilized on the ATR crystal as described in detail.[1]

Cyclic voltammetry and activation of C*c*O. Prior to infrared measurements, up to 80 cyclic voltammetry cycles were performed on the immobilized C*c*O under aerobic conditions to transfer the protein from the inactivated to the activated conformational state.[2,31] Electrochemical measurements were performed with a potentiostat from Autolab (PGSTAT12 with GPES 4.9 from Metrohm, Herisau, Switzerland) in a three-electrode configuration with gold as the working electrode, a Ag|AgCl,KCl_{sat} reference and a platinum wire as the counter electrode. All electrode potentials are quoted versus the standard hydrogen electrode (SHE). Cyclic voltammetry measurements were done in PBS solution (0.05 M K_2HPO_4, 0.1 M KCl, pH 8) flushed with O_2 and with vertex potentials V_1 = +400 mV and V_2 = -800 mV at a sweep

rate of 50 mVs^{-1}. As soon as the peak currents acquired constant positions and heights over a couple of cycles, indicating that the protein had been transferred to the activated conformational state,[2] the aerobic solution was exchanged with anaerobic PBS buffer. To establish anaerobic conditions, the PBS solution was flushed with argon for 20 minutes, after which a chemical oxygen trap consisting of glucose (0.3% w/w), glucose oxidase (75 µg/ml) and catalase (12.5 µg/ml) was added.

ATR-SEIRA-Spectroscopy. The electrochemical cell was mounted on top of a trapezoid single reflection silicon ATR crystal. The IR beam of the FTIR spectrometer (VERTEX 70v, from Bruker, Ettlingen, Germany) was coupled into the crystal at an angle of incidence Θ = 60° by using the custom-made setup described previously.[27] All spectra were measured with parallel polarized light. Because the ATR element surface is coated with an electrical conductor, perpendicularly polarized light is unable to penetrate the conducting layer effectively. The total reflected IR beam intensity was measured with a liquid nitrogen-cooled photovoltaic mercury cadmium telluride (MCT) detector. IR measurements were done under anaerobic conditions at 28 °C. The sample unit was purged with dry, carbon dioxide-free air. FTIR spectra were recorded at 4 cm^{-1} resolution using Blackham-Harris 3-term apodization and a zero filling factor of 2. Due to small sample absorbances of the protein monolayer beside the large absorbance of water, interferograms were measured in double-sided mode and transformed into spectra using the Power phase correction mode. An optical filter (LWP < 2.966 cm^{-1}) was used to reduce the high folding limit to 3159 cm^{-1} and consequently, the number of necessary interferogram points to 2842. Spectra were analyzed using the software package OPUS 6.5 and OriginLab's Origin software.[32]

Principle of tr-ATR-SEIRA-Spectroscopy triggered by electrochemical potentials. The rectangular waveform used for modulated excitation was provided by a function generator (Agilent 33250A, Santa Clara, CA, US) that triggered the Autolab potentiostat and

the spectrometer, as shown in Fig. 1. Potentials were periodically applied to the ptBLM on the gold film in the form of a square wave function to change the redox state of C*c*O from the fully oxidized (+400 mV) to the fully reduced state (-800 mV), as depicted in Fig. 2. Due to the charging of the Au/water interface, the range of potential actually affecting the enzyme lies between +200 mV and -600 mV.[33,34] FTIR measurements were triggered by the fast potential change at the start of each period to record a succession of spectra that indicate changes of IR absorbances as a function of time. Absorbances were calculated using the fully reduced state of the protein as a reference. Spectra were recorded at frequencies of 20 Hz (period = 50 ms, time-resolution = 1000 µs, 30 co-additions.), 50 Hz (20 ms, 400 µs, 75 co-adds.), 100 Hz (10 ms, 200 µs, 150 co-adds.), 250 Hz (4 ms, 80 µs, 370 co-adds.) and 500 Hz (2 ms, 40 µs, 700 co-adds.). These parameters result in 50 time slides per period for all excitation frequencies.

Principle of Phase Sensitive Detection (PSD). The analytical procedure of phase sensitive detection was applied to time-resolved spectra co-added during excitation cycles. PSD enables background elimination in absorbance spectra by separating the ac and dc components in the system response and by selectively detecting signals that respond t the fundamental frequency ω (i.e. excitation frequency) or higher harmonics.[3,4] PSD can be applied to systems that exhibit a reversible response to an external perturbation. In this study, PSD was used to improve the SNR of the measured spectra by distinguishing the weak system response of the protein monolayer from the large background absorption.

The time-dependent absorbance $A_i(\tilde{\nu},t)$ of all vibrational modes i can be described by Eq. 1,

$$A_i(\tilde{\nu},t) = \sum_{i=1}^{N} \left(A_{i,0}(\tilde{\nu}) + \sum_{k=1}^{\infty} A_{i,k}(\tilde{\nu}) \sin\left(k\omega t + \varphi_{i,k}\right) \right) \quad (1)$$

where k denotes the multiple of the fundamental ($k = 1$ fundamental frequency, $k > 1$ higher harmonics) and $\varphi_{i,k}$ indicates the phase lag of the k^{th} harmonic that is independent of the wavenumber and associated with the vibrational mode i. The left-hand part within the summation bracket corresponds to the stationary overall absorbance (dc-part) and the right-hand part corresponds to the modulated system response (ac-part). The phase-resolved absorbance spectrum $A_k^{\phi^{PSD}}(\tilde{\nu})$ with the operator-controlled phase angle ϕ_k^{PSD} is obtained by multiplication of $A_i(\tilde{\nu},t)$ by e.g. $\sin\left(k\omega t + \phi_k^{PSD}\right)$ followed by a normalized integration over the modulation period T. In this study, only the fundamental frequency ($k = 1$) was used for calculations. Therefore, k is omitted in all subsequent equations, and the phase-resolved absorbance spectrum of the fundamental is reduced to Eq. 2.

$$A^{\phi^{PSD}}(\tilde{\nu}) = \frac{2}{T}\int_0^T A_i(\tilde{\nu},t)\,\sin\left(\omega t + \phi^{PSD}\right)\mathrm{d}t \tag{2}$$

Straightforward calculation leads to Eq. 3, which describes the relation between the calculated phase-resolved spectrum, the searched amplitudes $A_i(\tilde{\nu})$ and the phase lags φ_i of the components i and where $A_i^{\phi^{PSD}}(\tilde{\nu})$ represents the phase-resolved absorbance of the vibrational mode i.

$$A^{\phi^{PSD}}(\tilde{\nu}) = \sum_{i=1}^{N} A_i^{\phi^{PSD}}(\tilde{\nu}) = \sum_{i=1}^{N} A_i(\tilde{\nu})\,\cos\left(\varphi_i - \phi^{PSD}\right) \tag{3}$$

As the absorbance of a single component will later be given by the evaluated peak area of the absorption of its vibrational mode (e.g. by curve-fitting) we can eliminate the dependency of the wavenumber using Eq. 4.

$$A_i = \int A_i(\tilde{\nu})\,\mathrm{d}\tilde{\nu} \tag{4}$$

Using Eq. 3 and 4, the wavenumber-independent phase-resolved absorbance of a vibrational mode *i* is then given by Eq. 5 as follows:

$$A^{\phi^{PSD}} = A_i \cos\left(\varphi_i - \phi^{PSD}\right) \tag{5}$$

Due to the characteristics of the cosine function, $A_i^{\phi^{PSD}}$ becomes maximum for $\varphi_i = \phi^{PSD}$, meaning that the absorbance of a component with the phase lag φ_i reaches its maximum in the phase-resolved spectrum with $\phi^{PSD} = \varphi_i$. This behavior permits the discrimination of overlapping bands (resulting from the absorbance of different components) in a set of phase-resolved spectra with the prerequisite that the phase lag of the selected bands is different. Therefore, the phase-resolved spectrum with $\phi^{PSD} = \varphi_i \pm 90$ results in zero absorbance for the vibrational mode A_i. A non-zero absorbance at this phase setting originates therefore only from other components.

As seen in Eq. 6, the tr-absorbance of one vibrational mode $A_i(t)$ can be expressed by $A_i^{0°}$ and $A_i^{90°}$, the phase-resolved spectra at $\phi^{PSD} = 0°$ and $\phi^{PSD} = 90°$, respectively

$$A_i(t) = \sum_{i=1}^{N} \left(A_i^{0°} \cos(\omega t) + A_i^{90°} \sin(\omega t) \right) \tag{6}$$

Finally, the amplitude and phase lag of the response of a vibrational mode are given by Eq. 7-9 and can therefore be calculated from the evaluated phase-resolved spectra $A_i^{0°}$ and $A_i^{90°}$.

$$A_i = \sqrt{A_i^{0°2} + A_i^{90°2}} \tag{7}$$

$$\cos\left(\varphi_i\right) = \frac{A_i^{0°}}{A_i}, \quad \sin\left(\varphi_i\right) = \frac{A_i^{90°}}{A_i} \tag{8}$$

$$\varphi_i = \arctan\left(\frac{A_i^{90°}}{A_i^{0°}}\right) \tag{9}$$

As depicted in Fig. 3, Eq. 8 can be combined to Eq. 9. However, because the result of the arctan function is only defined to be within -90° and 90°, the phase lags in the range of 0°–360° must be determined from Eq. 8 as reported by Baurecht et al..[3] We further assume the kinetic approach of Fringeli et al.,[4] which accounts for a reversible first-order reaction, whose rate constant is considered to change as a function of the magnitude of the excitation parameter. As a result, the relationship between the phase lag and the excitation frequency f is given by Eq. 10,

$$\tan(\varphi) = -2\pi f \tau_m \tag{10}$$

with the relaxation time τ_m.

Curve-fitting of PSD spectra. Curve-fitting of phase-resolved spectra was performed with OriginLab's Origin software[32] using the Levenberg-Marquardt algorithm and Lorentzian band shapes. In order to account for the modulated absorbance changes of abundant water molecules in the electric field, a H_2O-bending band ($\delta(H_2O)$) was added to the fit model. Therefore, fixed band parameters such as a band position of 1643 cm^{-1} and a full width at half maximum (FWHM) of 80 cm^{-1}, evaluated from an independently measured spectrum of pure H_2O. The phase lags of the separated components were calculated according to Eq. 9. The corresponding band areas $A_i^{\phi^{PSD}}(\omega)$ were determined by curve-fitting the phase-resolved spectra at $\phi^{PSD} = 0°$ and $\phi^{PSD} = 90°$ of all five excitation frequencies ω. Initial values for band positions and FWHM were estimated by visual inspection of phase-resolved spectra using several different angles ϕ^{PSD}. Due to the high number of free parameters, the upper and lower limits were set in the fitting software to ±2 cm^{-1} for band positions. At this point, all other parameters i.e. FWHM and intensity were allowed to be fitted by the program. This first curve fit of the 10 phase-resolved spectra resulted in a slightly varying number and position of bands for each spectrum. Thus, in the second iteration, only the band positions that occurred

in all fitted spectra (±1 cm^{-1}) were considered and averaged for further analysis, also FWHM values were averaged. Prior to the third iteration, bands that did not exhibit an increasing phase lag with increasing excitation frequency were excluded from the data set and the band position and FWHM values of the remaining components were retained. The final fit was performed by only allowing the band intensity to be fitted. Phase lags calculated using that method are phase lags related to the trigger signal.

RESULTS AND DISCUSSION

C*c*O from *Rhodobacter sphaeroides* was immobilized on a two-layer gold film[27] deposited on an ATR crystal and reconstituted into a protein-tethered bilayer lipid membrane (ptBLM). The enzyme was then transferred to its activated state by several cyclic voltammetry cycles. SEIRA spectra were acquired under strictly anaerobic conditions in the Step-Scan mode by applying periodic potential pulses stepping between -800 mV to +400 mV. As it has been shown previously,[25,35] electron transfer within C*c*O occurs in the millisecond time scale. In this work, excitation frequencies in the range from 20 to 500 Hz and time-resolutions in the millisecond time range were used. This ensures best conditions to detect changes of vibrational components involved in this process by PSD. Each excitation frequency was measured with a new sample of C*c*O reconstituted into the ptBLM system. Tr-SEIRA spectra obtained after baseline correction (Fig. 4a) featured a broad band in the amide I region, similar to the prominent bands obtained previously in potentiometric titration experiments followed by SEIRAS.[2] In titration spectra, band analysis with Two-Dimensional (2D) spectra proved to be successful. However, in tr-SEIRAS, the spectra contained many more overlapping bands in addition to a high level of noise as seen in Fig. 4a. For further analysis and band deconvolution, phase-resolved spectra were calculated at different phase settings

ϕ^{PSD} (Fig. 4b). The reduction of the noise in the PSD spectrum is immediately visible, because static signals as well as noise, that are not correlated to the modulation frequency, have been eliminated. This kind of noise reduction illustrates the advantage of PSD to other spectra evaluation techniques e.g. two-dimensional correlation spectroscopy, where static background and noise may distort the correlation spectra and therefore lead to inaccurate band assignments.[36,37]

The significant change in shape of the phase-resolved spectra at different phase angles clearly indicates the presence of several vibrational components with different phase lags, as outlined in the experimental section. Considering the bands at 1619.9 cm^{-1} and 1625.5 cm^{-1} in Fig. 4b, the absorbance of the first band is more prominent at the phase angle of 60° (bold green line), whereas the absorbance of the latter band is more pronounced at a 180° phase angle (bold blue line). Even though the improved SNR reveals a large number of potential analytical bands, the selection of the valid vibrational bands was exclusively accomplished by evaluation of the progression of phase lags with increasing excitation frequencies as discussed further below.

Only the spectral features of the amide I region that is known to be particularly sensitive for conformational changes in proteins[38] were used for evaluation of vibrational components by PSD in the present study. The relative phase lags of the single components were calculated according to Eq. 9 after curve fitting the 0° and 90° phase-resolved spectra. A representative curve fit is shown in Fig. 5a. In the course of the incremental fitting procedure, it became apparent that water molecules also respond to the modulated excitation. Numerous FT-IR studies of proteins were conducted in D_2O rather than in H_2O in order to avoid interference of the H_2O bending band with the amide I band. However, it was reported that exposure of proteins to D_2O leads to changes in structure[39] such as altered salt bridges[40] and protein denaturation,[41,42] as well as changes in their function,[43] particularly in proteins with internal

electron transfer.[44,45] Consequently, present measurements were carried out in aqueous buffer solution rather than D_2O buffer elsewhere used for FTIR investigations of proteins. Considering that the water molecule represents a strong dipole, small changes in orientation may have a significant impact on the IR spectrum. Effects on water bands by potential changes have been reported previously.[46,47]

Subtraction of H_2O bending bands in FTIR-spectra of proteins by the user is delicate, because it is prone to personal bias and uncertainty.[48] We believe that water subtraction by PSD is superior in this respect, because it is rather objective and free from the operator's judgement. For evaluation with PSD, water is treated as a species that responds to the potential modulation, and a fixed parameter set obtained by static IR measurements was included in the fitting procedure to account for the H_2O-bending band ($\delta(H_2O)$). As shown in Fig. 6, it shows the same phase lag increase as the other identified components.

The origin of the H_2O-bending band is assumed to be the water molecules in the submembrane space (i.e. the space between the membrane and the crystal) provided by the linker molecule in the ptBLM system.[1] The high absorbance of the H_2O-bending band in the ME-SEIRA spectra can be explained by an inherent characteristic of SEIRAS as the intensity of the surface-enhanced field in SEIRAS experiments decreases with the 6^{th} power of the distance from the crystal.[49] Therefore, vibrations of groups in the immediate vicinity of the ATR crystal yield a higher absorbance than vibrations of groups situated further away (at the same concentration of absorbing groups).

Subtraction of the $\delta(H_2O)$ band by PSD facilitates the evaluation of the absorbance of the components as shown in Fig. 5b in an example of the final fit result obtained from the 90° phase-resolved spectrum with a modulation frequency of 20 Hz. Fig. 5b clearly shows the low level of noise in the 10^{-4} AU range as compared to the absorbance of components. Positive and negative components in a phase-resolved spectrum indicate that phase lags of the

components are different in the range of 180° e.g. positive bands in the 0° phase-resolved spectra indicate that the band increases at the first excitation half-period, a negative band in the 0° phase-resolved spectra indicates a decrease, respectively. The phase lag, however, can only be determined by considering both, the 0° and 90° phase-resolved spectra according to Eq. 9. The phase lags of the vibrational components as a function of the excitation frequency are shown in Fig. 6. Theory predicts that (i) phase lags of the vibrational components increase with increasing excitation frequency, (ii) phase lags are located within the first and the third quadrant for the response of first-order reactions to modulated excitation and (iii) phase lags should be different for individual vibrational components. Only the components matching all of these criteria were considered significant. In addition to criterion (ii), since the response signal cannot increase while the excitation signal decreases, the phase lags cannot lie within the second and fourth quadrants. Components with phase lags in the third quadrant are in anti-phase compared to components in the first quadrant. At this point, it should be emphasized that due to the presence of the gold film evaporated on the ATR crystal, only the component of the transition dipole moments perpendicular to the metal surface can be detected.[50] Therefore, only changes in absorbance of vibrational modes with such components are observed. From Fig. 6, we can deduce that the phase lags are different for the individual vibrational components, as requested in (iii). In order to resolve individual vibrational components within an overlapping absorption band, it is essential that the difference in their phase lags is large. At relatively low frequencies, the difference of the phase lags is rather small, since all components (which have themselves faster reaction rates than the trigger) are able to respond immediately to the trigger. Therefore the amplitude of the changes is large in this frequency range. When the excitation frequencies become too high, the modulation amplitude decreases and all phase lags originating from the stimulation parameter end up at the same phase lag. Thus there is always an optimum frequency range where phase lags

become maximum in modulated excitation experiments.[4] This is in good agreement with the data shown in Fig. 6, where the largest difference of phase lags is between 50 – 250 Hz, with smaller differences at lower and higher excitation frequencies. Accordingly, the optimum frequency range for band separation in the measurements was deduced to be between 50 – 250 Hz. Finally, vibrational components were identified and associated band parameters were collected in Table 1. [51-54]

Although the primary aim of this work is to show the prospects of band separation by PSD, as a first insight into the kinetics of conformational changes, a fit for the progression of the obtained phase lags of every component with increasing excitation frequency is included in Fig. 6. The relation given in Eq. 10 only applies to a first-order reaction.[4] Since conformational changes due to electron transfer along redox centers exhibit kinetics of a higher order, in our study, Eq. 10 can only give a rough estimate of the phase lag progression with increasing excitation frequency. Nevertheless, some conclusions can be derived from that. For example, the band at 1690.4 cm^{-1} in the first quadrant exhibits the smallest phase lag. This band can be assigned to the C=O stretching vibration, characteristic for β-sheets and has been tentatively attributed to changes in the Cu_A-redox center. Because this redox center is the first in the native electron pathway within the C*c*O, it is conceivable that Cu_A is reduced by the electrochemical excitation prior to the ensuing redox centers. Moreover, increased flexibility of the β-sheet region has been shown by computational methods,[55,56] and has been confirmed by deuterium exchange analysis.[57] In the third quadrant, the band at 1596.5 cm^{-1} is the vibrational component with the lowest phase lag. This band has been assigned to one of the histidine residues of the porphyrin ring of heme *a*, which is the second electron center in C*c*O and the direct successor of Cu_A. Within the margin of error, the band with the next higher phase lag is the band at 1643.0 cm^{-1},which has been assigned to water. The H_2O-

bending band is expected to have a small phase lag, because it is a small molecule and does not participate in protein dynamics.

CONCLUSION

In the present study, C*c*O was stimulated by modulated electrochemical excitation while simultaneously performing SEIRAS in the Step-Scan mode. Overlapping structural bands in tr-SEIRA spectra were deconvoluted and separated from large background noise by rigorous application of the analytical procedure of PSD. Hence, enhancement of SNR permitted the identification of vibrational components in the amide I region. Crucial in this context has been the elimination of the large water band present beneath the amide I band. Evaluation of phase lags revealed the characteristic increase with increasing excitation frequency. This inherent validation proved PSD to be superior to other band-identification techniques such as FSD or first-order derivative which depend significantly on the operator choice of initial parameters, while evaluation by PSD is based on standard analytical procedures and validated by theoretical constraints. The bands assigned to secondary structures can also be attributed to specific redox centers. After application of PSD to tr-SEIRA spectra of cytochrome *c*[11] and C*c*O, our group showed that this method is an excellent tool for band deconvolution and identification of modulated-excitation FTIR spectra. Further analysis of tr-SEIRA spectra of C*c*O with respect to redox kinetics will be presented in the near future.[34]

ACKNOWLEDGEMENTS

We gratefully acknowledge the invaluable advice and assistance of Prof. Dieter Baurecht, Institute of Physical Chemistry, University of Vienna, Austria. Partial support for this work was provided by ZIT, Center of Innovation and Technology of Vienna.

REFERENCES

1. C. Nowak, D. Schach, J. Gebert, M. Grosserueschkamp, R.B. Gennis, S. Ferguson-Miller, W. Knoll, D. Walz, R.L.C. Naumann. "Oriented immobilization and electron transfer to the cytochrome c oxidase". J. Solid State Electrochem. 2011. 15(1): 105-114.
2. C. Nowak, M.G. Santonicola, D. Schach, J. Zhu, R.B. Gennis, S. Ferguson-Miller, D. Baurecht, D. Walz, W. Knoll, R.L.C. Naumann. "Conformational transitions and molecular hysteresis of cytochrome c oxidase: Varying the redox state by electronic wiring". Soft Matter 2010. 6(21): 5523-5532.
3. D. Baurecht, U.P. Fringeli. "Quantitative modulated excitation Fourier transform infrared spectroscopy". Rev. Sci. Instrum. 2001. 72(10): 3782-3792.
4. U.P. Fringeli, D. Baurecht, H.H. Günthard. "Biophysical Infrared Modulation Spectroscopy". In: H. U. Gremlich and B. Yan, editors. Infrared and Raman Spectroscopy of Biological Materials New York: Marcel Dekker, 2001. pp. 143-192.
5. D. Baurecht, I. Porth, U.P. Fringeli. "A new method of phase sensitive detection in modulation spectroscopy applied to temperature induced folding and unfolding of RNase A". Vib. Spectrosc. 2002. 30(1): 85-92.
6. M. Muller, R. Buchet, U.P. Fringeli. "2D-FTIR ATR spectroscopy of thermo-induced periodic secondary structural changes of poly-(L)-lysine: A cross-correlation analysis of phase-resolved temperature modulation spectra". J. Phys. Chem. 1996. 100(25): 10810-10825.
7. M. Bieri, T. Burgi. "L-Glutathione chemisorption on gold and acid/base induced structural changes: A PM-IRRAS and time-resolved in situ ATR-IR spectroscopic study". Langmuir 2005. 21(4): 1354-1363.

8. T. Burgi, A. Baiker. "In situ infrared spectroscopy of catalytic solid-liquid interfaces using phase-sensitive detection: Enantioselective hydrogenation of a pyrone over Pd/TiO2". J. Phys. Chem. B 2002. 106(41): 10649-10658.
9. D. Baurecht, G. Reiter, N. Hassler, M. Schwarzott, U.P. Fringeli. "Application of Special FTIR ATR Techniques for Quantitative Structural Analysis of Thin Surface Layers". Chimia 2005. 59226-235.
10. M. Schwarzott, P. Lasch, D. Baurecht, D. Naumann, U.P. Fringeli. "Electric field-induced changes in lipids investigated by modulated excitation FTIR spectroscopy". Biophys. J. 2004. 86(1): 285-295.
11. C. Nowak, C. Luening, D. Schach, D. Baurecht, W. Knoll, R.L.C. Naumann. "Electron Transfer Kinetics of Cytochrome C in the Submillisecond Time Regime Using Time-Resolved Surface-Enhanced Infrared Absorption Spectroscopy". J. Phys. Chem. C 2009. 113(6): 2256-2262.
12. I. Noda, G.M. Story, C. Marcott. "Pressure-induced transitions of polyethylene studied by two-dimensional infrared correlation spectroscopy". Vib. Spectrosc. 1999. 19(2): 461-465.
13. Q. Wu, X. Lu, S. Yang, B. Zhang. "Dynamic double modulation with step scan FTIR spectroscopy on polyurethane film". Spectrosc. Spect. Anal. 2002. 22(1): 25-28.
14. M. Forster, K. Loth, M. Andrist, U.P. Fringeli, H.H. Günthard. "Kinetic study of the photooxidation of pyrocatechol by modulated electronic excitation IR and ESR spectroscopy (MEIR and MESR)". Chem. Phys. 1976. 17(1): 59-80.
15. R. Wirz, T. Burgi, A. Baiker. "Probing enantiospecific interactions at chiral solid-liquid interfaces by absolute configuration modulation infrared spectroscopy". Langmuir 2003. 19(3): 785-792.

16. R. Wirz, T. Burgi, W. Lindner, A. Baiker. "Absolute configuration modulation attenuated total reflection IR spectroscopy: An in situ method for probing chiral recognition in liquid chromatography". Anal. Chem. 2004. 76(18): 5319-5330.
17. J.A. Bailey, F.L. Tomson, S.L. Mecklenburg, G.M. MacDonald, A. Katsonouri, A. Puustinen, R.B. Gennis, W.H. Woodruff, R.B. Dyer. "Time-resolved step-scan Fourier transform infrared spectroscopy of the CO adducts of bovine cytochrome c oxidase and of cytochrome bo(3) from Escherichia coli". Biochemistry 2002. 41(8): 2675-2683.
18. D. Heitbrink, H. Sigurdson, C. Bolwien, P. Brzezinski, J. Heberle. "Transient Binding of CO to CuB in Cytochrome c Oxidase Is Dynamically Linked to Structural Changes around a Carboxyl Group: A Time-Resolved Step-Scan Fourier Transform Infrared Investigation". Biophys. J. 2002. 82(1): 1-10.
19. E. Pinakoulaki, U. Pfitzner, B. Ludwig, C. Varotsis. "The role of the cross-link His-Tyr in the functional properties of the binuclear center in cytochrome c oxidase". J. Biol. Chem. 2002. 277(16): 13563-13568.
20. S. Stavrakis, K. Koutsoupakis, E. Pinakoulaki, A. Urbani, M. Saraste, C. Varotsis. "Decay of the Transient CuB−CO Complex Is Accompanied by Formation of the Heme Fe−CO Complex of Cytochrome cbb3−CO at Ambient Temperature: Evidence from Time-Resolved Fourier Transform Infrared Spectroscopy". J. Am. Chem. Soc. 2002. 124(15): 3814-3815.
21. C. Koutsoupakis, E. Pinakoulaki, S. Stavrakis, V. Daskalakis, C. Varotsis. "Time-resolved step-scan Fourier transform infrared investigation of heme-copper oxidases: implications for O2 input and H2O/H+ output channels". Biochim. Biophys. Acta, Bioenerg. 2004. 1655347-352.

22. R.M. Nyquist, D. Heitbrink, C. Bolwien, R.B. Gennis, J. Heberle. "Direct observation of protonation reactions during the catalytic cycle of cytochrome c oxidase". Proc. Natl. Acad. Sci. U.S.A. 2003. 100(15): 8715-8720.
23. D. Okuno, T. Iwase, K. Shinzawa-Itoh, S. Yoshikawa, T. Kitagawa. "FTIR Detection of Protonation/Deprotonation of Key Carboxyl Side Chains Caused by Redox Change of the CuA-Heme a Moiety and Ligand Dissociation from the Heme a3-CuB Center of Bovine Heart Cytochrome c Oxidase". J. Am. Chem. Soc. 2003. 125(24): 7209-7218.
24. B. Rost, J. Behr, P. Hellwig, O.M.H. Richter, B. Ludwig, H. Michel, W. Mantele. "Time-resolved FT-IR studies on the CO adduct of Paracoccus denitrificans cytochrome c oxidase: Comparison of the fully reduced and the mixed valence form". Biochemistry 1999. 38(23): 7565-7571.
25. B.H. McMahon, M. Fabian, F. Tomson, T.P. Causgrove, J.A. Bailey, F.N. Rein, R.B. Dyer, G. Palmer, R.B. Gennis, W.H. Woodruff. "FTIR studies of internal proton transfer reactions linked to inter-heme electron transfer in bovine cytochrome c oxidase". Biochim. Biophys. Acta, Bioenerg. 2004. 1655(1-3): 321-331.
26. F. Tomson, J.A. Bailey, R.B. Gennis, C.J. Unkefer, Z.H. Li, L.A. Silks, R.A. Martinez, R.J. Donohoe, R.B. Dyer, W.H. Woodruff. "Direct infrared detection of the covalently ring linked His-Tyr structure in the active site of the heme-copper oxidases". Biochemistry 2002. 41(48): 14383-14390.
27. C. Nowak, C. Luening, W. Knoll, R.L.C. Naumann. "A Two-Layer Gold Surface with Improved Surface Enhancement for Spectro-Electrochemistry Using Surface-Enhanced Infrared Absorption Spectroscopy". Appl. Spectrosc. 2009. 63(9): 1068-1074.
28. F. Giess, M. Friedrich, J. Heberle, R. Naumann, W. Knoll. "The Protein-Tethered Lipid Bilayer: A Novel Mimic of the Biological Membrane". Biophys. J. 2004. 87(5): 3213-3220.

29. D. Schach, C. Nowak, R.B. Gennis, S. Ferguson-Miller, W. Knoll, D. Walz, R.L.C. Naumann. "Modeling direct electron transfer to a multi-redox center protein: Cytochrome c oxidase". J. Electroanal. Chem. 2010. 649(1-2): 268-276.
30. K. Ataka, F. Giess, W. Knoll, R. Naumann, S. Haber-Pohlmeier, B. Richter, J. Heberle. "Oriented Attachment and Membrane Reconstitution of His-Tagged Cytochrome c Oxidase to a Gold Electrode: In Situ Monitoring by Surface-Enhanced Infrared Absorption Spectroscopy". J. Am. Chem. Soc. 2004. 126(49): 16199-16206.
31. M.G. Friedrich, J.W.F. Robertson, D. Walz, W. Knoll, R.L.C. Naumann. "Electronic Wiring of a Multi-Redox Site Membrane Protein in a Biomimetic Surface Architecture". Biophys. J. 2008. 94(9): 3698-3705.
32. OriginPro 8.6G, v8.6.0 SR3. OriginLab, Northampton, 2012.
33. D. Schach, Direct Electron Transfer to the Cytochrome c Oxidase investigated by Electrochemistry and Time-Resolved Surface-Enhanced Infrared Absorption Spectroscopy, Ph.D. Thesis (Johannes Gutenberg Universität Mainz, Mainz, 2011).
34. A. Schwaighofer, C. Steininger, D.M. Hildenbrandt, J. Srajer, C. Nowak, W. Knoll, R.L.C. Naumann. "Time-Resolved Surface-Enhanced IR-Absorption Spectroscopy of direct Electron Transfer to Cytochrome c Oxidase from R. sphaeroides". Biophys. J. 2013. under review
35. P. Brzezinski. "Internal Electron-Transfer Reactions in Cytochrome c Oxidase". Biochemistry 1996. 35(18): 5611-5615.
36. Z.W. Yu, J. Liu, I. Noda. "Effect of noise on the evaluation of correlation coefficients in two-dimensional correlation spectroscopy". Applied Spectroscopy 2003. 57(12): 1605-1609.
37. M.A. Czarnecki. "Interpretation of two-dimensional correlation spectra: Science or art?". Applied Spectroscopy 1998. 52(12): 1583-1590.

38. J.L.R. Arrondo, A. Muga, J. Castresana, F.M. Goñi. "Quantitative studies of the structure of proteins in solution by fourier-transform infrared spectroscopy". Prog. Biophys. Mol. Biol. 1993. 59(1): 23-56.
39. D.K. Das, T. Mondal, U. Mandal, K. Bhattacharyya. "Probing Deuterium Isotope Effect on Structure and Solvation Dynamics of Human Serum Albumin". ChemPhysChem 2011. 12(4): 814-822.
40. A. Barth. "Infrared spectroscopy of proteins". Biochim. Biophys. Acta, Bioenerg. 2007. 1767(9): 1073-1101.
41. J.L.R. Arrondo, F.M. Goñi. "Structure and dynamics of membrane proteins as studied by infrared spectroscopy". Prog. Biophys. Mol. Biol. 1999. 72(4): 367-405.
42. E. Rial, A. Muga, J.M. Valpuesta, J.-L.R. Arrondo, F.M. Goñi. "Infrared spectroscopic studies of detergent-solubilized uncoupling protein from brown-adipose-tissue mitochondria". Eur. J. Biochem. 1990. 188(1): 83-89.
43. A. Kohen, H.H. Limbach. Isotope Effects In Chemistry and Biology. Boca Raton: CRC Press, 2005.
44. R.P. Sheridan, E.T. Knight, L.C. Allen. "The effect of deuterium substitution on hydrogen bonds in redox proteins". Biopolymers 1984. 23(2): 195-200.
45. O. Farver, J.D. Zhang, Q.J. Chi, I. Pecht, J. Ulstrup. "Deuterium isotope effect on the intramolecular electron transfer in Pseudomonas aeruginosa azurin". Proc. Natl. Acad. Sci. U.S.A. 2001. 98(8): 4426-4430.
46. K. Ataka, T. Yotsuyanagi, M. Osawa. "Potential-dependent reorientation of water molecules at an electrode/electrolyte interface studied by surface-enhanced infrared absorption spectroscopy". J. Phys. Chem. 1996. 100(25): 10664-10672.

47. M. Osawa, A. Yamakata. "Structure and Behavior of Water at the Electrochemical Interface Studied by Surface-Enhanced Infrared Absorption Spectroscopy". Jpn. Anal. 2011. 60(1): 1-9.
48. J.R. Powell, F.M. Wasacz, R.J. Jakobsen. "An Algorithm for the Reproducible Spectral Subtraction of Water from the Ft-Ir Spectra of Proteins in Dilute-Solutions and Adsorbed Monolayers". Appl. Spectrosc. 1986. 40(3): 339-344.
49. M. Osawa. "Dynamic Processes in Electrochemical Reactions Studied by Surface-Enhanced Infrared Absorption Spectroscopy (SEIRAS)". Bull. Chem. Soc. Jpn. 1997. 702861-2880.
50. M. Osawa, K. Ataka, K. Yoshii, Y. Nishikawa. "Surface-Enhanced Infrared-spectroscopy-The Origin of the Absorption Enhancement and Band Selection rule in Infrared-spectra of Molecules adsorbed on fine Metal Particles". Appl. Spectrosc. 1993. 47(9): 1497-1502.
51. E.A. Gorbikova, K. Vuorilehto, M. Wikstrom, M.I. Verkhovsky. "Redox titration of all electron carriers of cytochrome c oxidase by Fourier transform infrared spectroscopy". Biochemistry 2006. 45(17): 5641-5649.
52. P. Hellwig, S. Grzybek, J. Behr, B. Ludwig, H. Michel, W. Mantele. "Electrochemical and Ultraviolet/Visible/Infrared Spectroscopic Analysis of Heme a and a3 Redox Reactions in the Cytochrome c Oxidase from Paracoccus denitrificans: Separation of Heme a and a3 Contributions and Assignment of Vibrational Modes". Biochemistry 1999. 38(6): 1685-1694.
53. E. Goormaghtigh, V. Cabiaux, J.-M. Ruysschaert. "Secondary structure and dosage of soluble and membrane proteins by attenuated total reflection Fourier-transform infrared spectroscopy on hydrated films". Eur. J. Biochem. 1990. 193(2): 409-420.
54. B. Stuart. Biological Applications of Infrared Spectroscopy. New York: Wiley, 1997.

55. L. Qin, J. Liu, D.A. Mills, D.A. Proshlyakov, C. Hiser, S. Ferguson-Miller. "Redox-Dependent Conformational Changes in Cytochrome c Oxidase Suggest a Gating Mechanism for Proton Uptake". Biochemistry 2009. 48(23): 5121-5130.
56. L. Buhrow, S. Ferguson-Miller, Leslie A. Kuhn. "From Static Structure to Living Protein: Computational Analysis of Cytochrome c Oxidase Main-chain Flexibility". Biophys. J. 2012. 102(9): 2158-2166.
57. L.S. Busenlehner, L. Salomonsson, P. Brzezinski, R.N. Armstrong. "Mapping protein dynamics in catalytic intermediates of the redox-driven proton pump cytochrome coxidase". Proc. Natl. Acad. Sci. U.S.A. 2006. 103(42): 15398-15403.

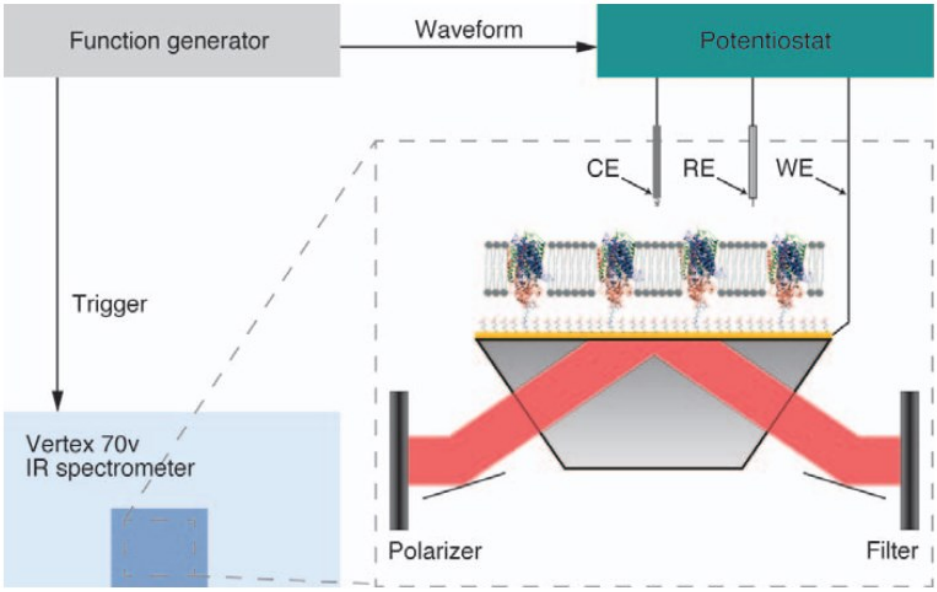

FIG 1. Setup for modulated excitation SEIRAS. The function generator provides the waveform that is applied to the protein layer by the potentiostat. Simultaneously, a trigger signal synchronizes the tr-SEIRAS measurements (CE: counter electrode, RE: reference electrode, WE: working electrode).

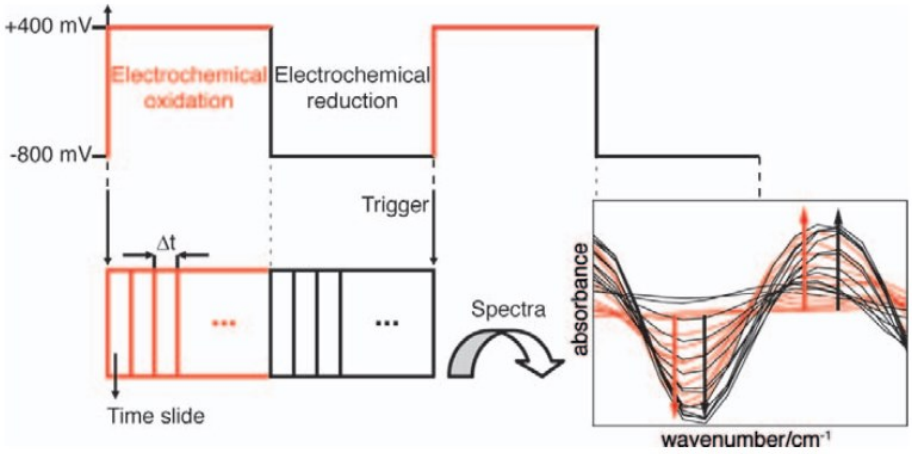

FIG 2. Principle of tr-SEIRAS measurements triggered by potential pulses. The trigger signal synchronizes the Step-Scan IR measurements and the beginning of each excitation period (potential jump from -800 mV to +400 mV). The relation between excitation frequency f, time-resolution Δt and number of time slides N_{TS} is given by $1/f = N_{TS} * \Delta t$.

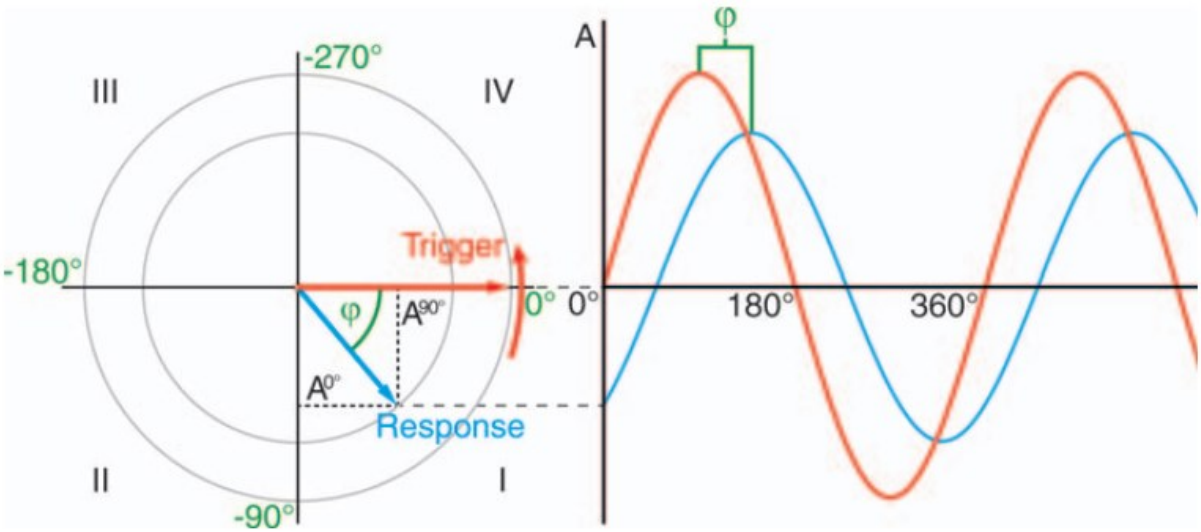

FIG 3. Schematic representation of the relationship between the excitation trigger (red), response signal (blue) and relative phase lag (green). The relative phase lag is indicated in negative digits, because the response exclusively occurs after the excitation. One excitation period is divided into 4 quadrants (roman numerals) in the polar coordinate system and the response vector of first-order reactions can only appear in the first and third quadrants (see text for details).

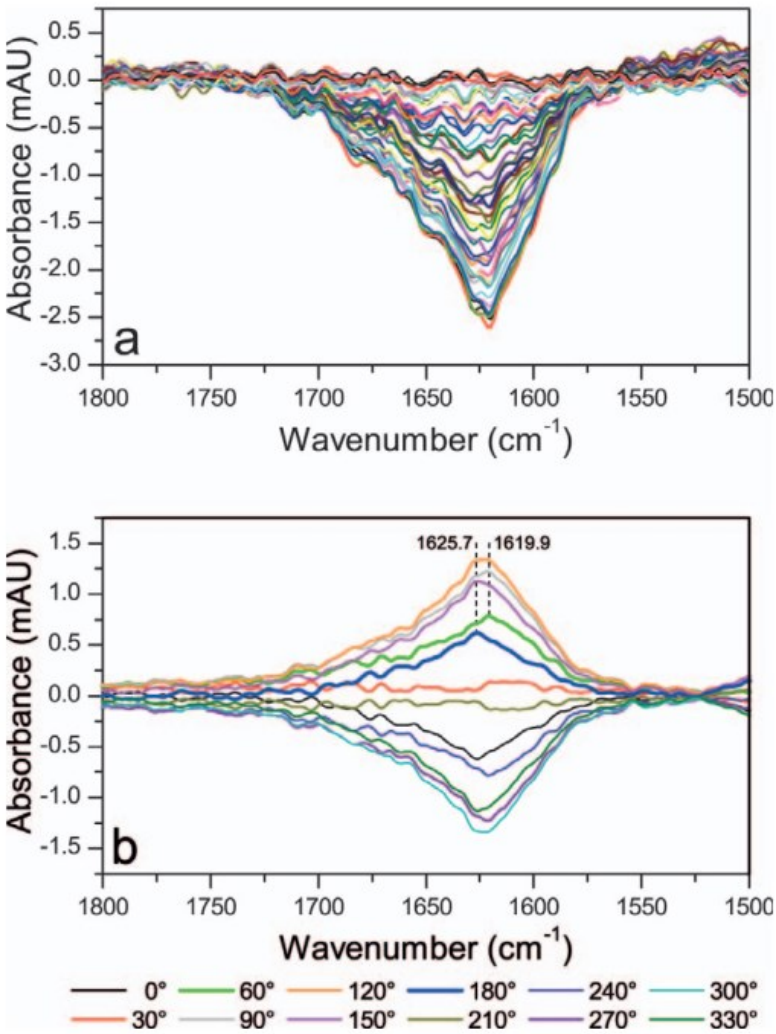

FIG 4. (**a**) Time-resolved and (**b**) phase-resolved FTIR-ATR absorbance spectra of the amide I region recorded with a modulation frequency of 100 Hz. The absorbance of the amide II band of the immobilized proteins was 2-2.5 mAU. (**a**) Tr-absorbance spectra were calculated using the fully reduced spectrum (first time slide) as reference. All 49 absorbance time slides are shown. (**b**) Phase-resolved spectra of the fundamental frequency with ϕ^{PSD}= 0,30,…,330°. The presence of different vibrational components at a certain wavenumber is indicated by a change of the band shape at different phase angles. Considering the bands at 1619.9 cm^{-1} and 1625.7 cm^{-1}, the absorbance of the first band is more pronounced at the phase angle of 60° (bold green line), while the absorbance of the latter band is more prominent at a phase angle of 180° (bold blue line).

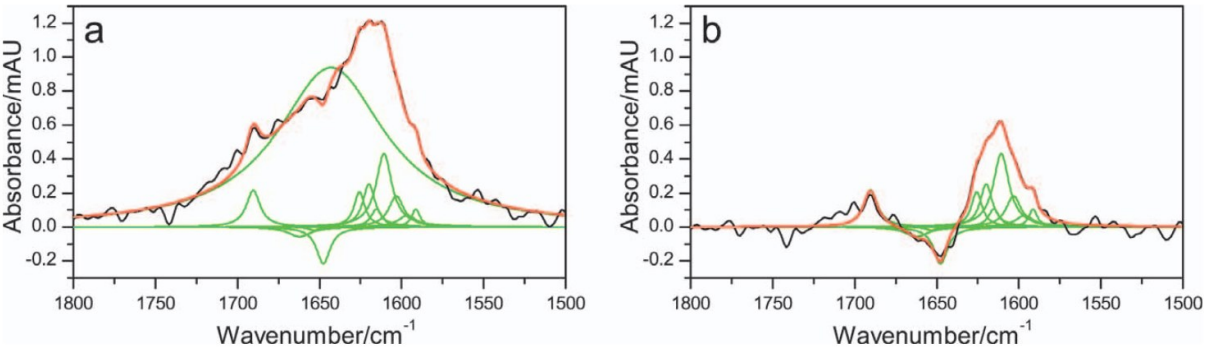

FIG 5. Curve fit of the 90° phase-resolved spectrum recorded with a modulation frequency of 20 Hz (**a**) with and (**b**) without the fitted water band (black: phase-resolved spectrum, green: curve-fitted vibrational components, red: sum of fitted components). The broad band in (**a**) with a maximum at 1643 cm^{-1} has been tentatively assigned to the H_2O-bending band. Positive and negative components within one phase-resolved spectrum appear when phase lags of the components are different in the range of 180°, e.g. one component increases and the other component decreases with increasing excitation parameter. In the region between 1700 cm^{-1} and 1750 cm^{-1}, bands could be fitted at certain phase-resolved spectra, but were excluded from the final parameter set because they did not show an increasing phase lag with increasing excitation frequencies.

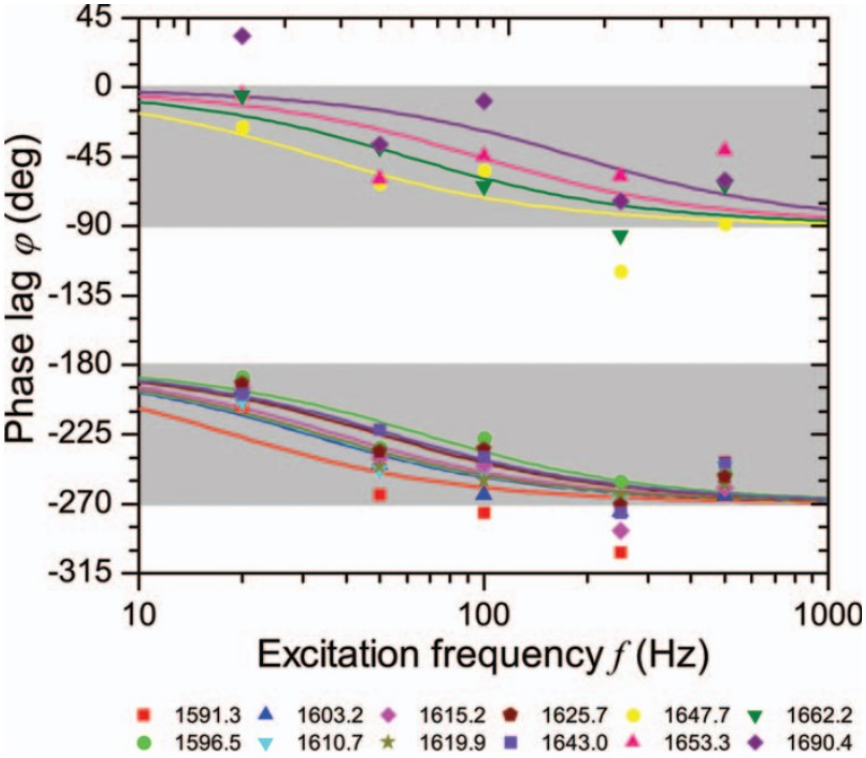

FIG. 6. Evaluated phase lags of the separated vibrational components in the amide I region. The lines indicate the progression of the phase lag with increasing excitation frequency by fitting the Eq. 10 to the data points. Grey areas indicate the first (0° – -90°) and third (-180° – -270°) quadrant as depicted in Fig. 3.

TABLE 1. Band parameters calculated by the fitting procedure and tentative band assignments of the evaluated vibrational components. (Numeration of the amino acid side chains refers to C*c*O from *Paracoccus denitrificans*). Band positions were allowed to vary within the margin of ±1cm^{-1}.

Experimental		Literature			
band position [cm^{-1}]	FWHM [cm^{-1}]	band position [cm^{-1}]	redox center	tentative band assignment	Ref.
1591.3	6.2	1592	Cu_A	H, HisH; ν(C═C); H224, H181/R, Arg-H_5^+; $\nu_{as}(CN_3H_5^+)$; R473/D; Asp-COO^-; $\nu_{as}(COO^-)$; D178	51
1596.5	13.4	1594	heme *a*	His	52
1603.2	11.3	1603	Cu_A	amide I (β-sheet); ν(C═O)	51
1610.7	11.7	1606	heme *a*	ν(C═O) CHO heme *a*; ν_7 heme *a*; ring O^- Tyr	52
1615.2	8.1	1637-1613	---	amide I (β-sheet)	53
1619.9	9.1	1618	heme a_3	Y, Tyr-OH; ν(CC) ring; δ(CH); Y280/W; ν(CC), ν(C═C); W272, W164/vinyl; ν(C-C) /amide I (β-sheet), ν(C═O)	51
		1618	heme *a*/ heme a_3	$\nu(C_\alpha{=}C_\beta)$ vinyl group (heme a/a_3); amide I (β-sheet)	52
1625.7	8.0	1630	heme a_3	R, Arg-H_5^+; $\nu_s(CN_3H_5^+)$; R473/H, $HisH_2^+$; ν(C═C); H403/formyl; amide I (β-sheet); ν(C═O)	51
1643.0	80.0	1645	---	δ(HOH)	54
1647.7	10.1	1651	Cu_A	amide I (α-helical); ν(C═O)	51
1653.3	8.0	1655	heme a_3	amide I (α-helical); ν(C═O)	51
		1656	heme a_3	amide I (α-helical)	52
1662.2	16.4	1661	heme *a*	amide I (α-helical), ν(C═O)/amide I, turns; ν(C═O)	51
		1662	heme *a*/ heme a_3	ν(C═O) CHO-heme a_3; amide I (α-helical); $\nu_{as}(CN_3H_5)$ Arg	52
1690.4	10.3	1689	Cu_A	amide I (β-sheet); ν(C═O)	51